

STRICT LIMITS ON THE IONIZING LUMINOSITY IN NGC 1068 FROM JET-AXIS MOLECULAR CLOUDS

J. Bland-Hawthorn and S.L. Lumsden
Anglo-Australian Observatory

G.M. Voit
Johns Hopkins University

G.N. Cecil
University of North Carolina

J.C. Weisheit
Rice University

ABSTRACT

The radio jet axis of NGC 1068 is characterised by energetic activity from x-ray to radio wavelengths. Detailed kinematic and polarization studies have shown that this activity is confined to bipolar cones centered on the AGN which intersect the plane of the disk. Thus, molecular clouds at 1 kpc distance along this axis are an important probe of the nuclear ionizing luminosity and spectrum. Extended $10.8\mu\text{m}$ emission coincident with the clouds is reasonably understood by dust heated to high temperatures by the nuclear radiation field. This model predicts that the nuclear spectrum is quasar-like (power law + blue excess) with a luminosity 2–5 times higher than inferred by Pier *et al.* (1994). Consequently, there is little or no polyaromatic hydrocarbon (PAH) emission associated with the radio-axis molecular clouds. We review this model in the light of new observations. A multi-waveband collage is included to illustrate the possible orientations of the double cones to our line of sight and the galaxian plane.

1. INTRODUCTION

The luminous Seyfert 2 galaxy NGC 1068¹ lies at the forefront of attempts to unify the broader class of “active galaxies” within a single physical framework (Antonucci & Miller 1985). One of the major uncertainties is the unobscured ionizing luminosity and spectrum of the active nucleus. Fortuitously, the axes of the anisotropic radiation cone and radio jet are inclined at roughly 45° to the plane of the disk (Cecil *et al.* 1990; Gallimore *et al.* 1994), such that the disk interstellar medium to the NE and SW sees the nuclear radiation field directly. Notably, Pogge (1988) and Bergeron *et al.* (1989) find that highly ionized species (e.g. O^{++} , Ne^{++} , Ne^{4+}) are confined to a fan-shaped region aligned with the radio axis.

The inner 3 kpc region (Fig. 2*a,b*) is dominated by a stellar bar aligned NE–SW (Scoville *et al.* 1988; Thronson *et al.* 1989) and by molecular spiral arms which begin at the ends of the bar (Planesas *et al.*

¹Unless otherwise stated, global quantities for NGC 1068 are taken from the Ringberg Standard (Bland-Hawthorn *et al.* 1997).

1991). In Fig. 2*a*, mid-infrared plumes (Telesco & Decher 1980) are coincident with the molecular clouds at 1 kpc radius, and have the same angular extent as the cones traced out by the [OIII] emission (Fig. 2*c*) and by soft x-rays (Fig. 2*d*). Here, we investigate the possibility that the extended mid-infrared emission arises from nuclear EUV/x-ray heating of dust grains on the surface of molecular clouds.

2. THE ORIENTATION OF THE IONIZATION CONES TO THE GALAXY DISK

We emphasize that, like the double radio source, the ionizing photons are escaping along bipolar cones. There is clear evidence that the NE cone illuminates the nearside of the disk, whereas the SW cone illuminates the farside, as illustrated in Fig. 1. In Fig. 3*b*, the line profiles throughout the bright NE plume are narrow compared to line profiles in the diffuse emission between plumes. This is easily understood if the bright emission arises from the surfaces of dense filaments, whereas the faint emission is associated with the ‘diffuse ionized medium’ (DIM) from a vertically extended medium throughout the inner disk (Bland-Hawthorn *et al.* 1991). In support of this picture, the [OIII] plumes coincide with dense molecular gas (e.g. Fig. 3*a*). Moreover, the NE plume (Fig. 2*c*) is remarkably similar to the SW plume if one makes allowances for extinction by the disk ($A_V \approx 2$); their locations are exactly bisymmetric with respect to the AGN. Note also how the [OIII] emission to the SW is completely blocked by the CO ring.

The same phenomenon explains the asymmetry in the x-rays although the extinction is more severe (Fig. 2*d*). To determine the opacity in the ROSAT bandpass, we write

$$\begin{aligned} \tau_{\text{ROSAT}} &= \sum_{\text{ions}} N_i \sigma_i(\varepsilon) & (1) \\ &= A_V (420/\varepsilon)^3 p & (2) \end{aligned}$$

where $p = [1 + \dots]$ indicates higher order terms (Brown & Gould 1976), i denotes different ions, N_i is the ion column density, and σ_i is the absorption cross-section as a function of energy ε in eV. For the range 0.1–0.5 keV, He absorption dominates the cross-section, while oxygen dominates in the range 0.5–2.4 keV; the bracketed terms are $p \approx 3$ and $p \approx 12$ respectively. Thus, τ_{ROSAT} lies in the range $1.5A_V$ to $3A_V$. We suspect that the soft x-rays also arise from filament surfaces as is well established in the M82 outflow (e.g. Shoppell & Bland-Hawthorn 1997).

3. THE MID-INFRARED EMISSION

Telesco & Decher (1988) found that almost all of the off-nucleus $10.8\mu\text{m}$ emission occurs in two diametric ‘plumes’ at roughly $15''$ radius along a NE–SW direction. The mid-infrared emission is clearly associated with the dense CO arms (Planesas *et al.* 1991), and shows some association with two of the brightest HII region complexes in the region scanned by the bolometer (Fig. 2*e*). But the excitation of these complexes is anomalous and shows evidence for ionization from the central source (Evans & Dopita 1986). Moreover, we note that strong $10.8\mu\text{m}$ emission is not detected in the NE complex (radius $\approx 25''$) nor in the NW complex at $10''$ radius, both of which fall within the scanned region. The NW complex is the brightest source of UV emission outside of the circumnuclear region (Neff *et al.* 1994). Once again, we

suspect that the MIR emission arises mostly from the skin of the clouds. Here, the NE and SW plumes are similar in flux density and morphology because the extinction is negligible at mid-infrared wavelengths.

From a reanalysis of VLA 6cm data (Wynn-Williams *et al.* 1985), we find little correlation between the $10.8\mu\text{m}$ emission and the underlying $\lambda\lambda 2 - 20\text{cm}$ continuum (Fig. 2*f*). When compared with HII regions, the ratio of $10.8\mu\text{m}$ to radio cm bands is high (20 – 50). Thronson, Campbell & Harvey (1978) find a tight relation between $11\mu\text{m}$ and cm-wave flux densities for high surface brightness galactic HII regions and molecular cloud complexes. They find $S_\nu(11\mu\text{m})/S_\nu(\text{cm}) = 10 \pm 3$ for a sample of ~ 40 objects. In larger HII region complexes and starburst galaxies, the synchrotron emission starts to overwhelm the free-free emission at around $\lambda 2\text{ cm}$ (Condon & Yin 1990), primarily because the star forming regions are now sufficiently large that stars are not able to migrate out of the region by the time they reach the supernova stage.

4. DUST GRAIN HEATING

Voit (1991; 1992) has considered how high energy photons heat and evaporate dust grains in molecular clouds. We now use the models to examine the possible impact of the Seyfert nucleus on molecular gas along the radio axis in NGC 1068. Mathis, Rumpl & Nordsieck (1977; MRN) have presented a dust grain model that successfully explains the ‘standard’ extinction curve in terms of the absorption and scattering properties of graphite and silicates. We adopt their power-law distribution of grain sizes, $dn = (A_{\text{Si}} + A_{\text{C}}) n_H a^{-3.5} da$, in the range $5\text{\AA} \leq a \leq 0.5\mu\text{m}$ normalized to the gas density, n_H . The abundances for the silicates, A_{Si} , and for graphite, A_{C} , assumed to be 100% carbon, are given elsewhere (Voit 1991).

At a distance of 1 kpc from the AGN, the projected mass of gas corresponds to $N_H \sim 1.2 \times 10^{23} \text{ cm}^{-2}$. For a Galactic dust to gas ratio, half of the total power in x-rays is absorbed by the dust and then re-radiated in the infrared. The remaining half absorbed by gas-phase atoms excites an equivalent luminosity in UV radiation which also heats the dust grains. Voit (1991) finds that most of the grains are opaque to UV radiation, while being translucent to x-rays. Since most of the surface area of the MRN composition lies in the small grains, these are predominantly UV heated. The x-rays require a significant stopping column and therefore heat the large grains preferentially. The temperature distribution of the grains directly determines the form of the re-radiated spectrum. The smallest grains, after absorbing individual photons, can superheat to temperatures more than an order of magnitude higher than their equilibrium temperatures (Puget & Leger 1989) before cooling down again. These ‘flickering grains’ give rise to broad temperature distributions. X-ray photons can evaporate small grains ($a \leq 10\text{\AA}$) on a very short timescale through repeated superheating to temperatures in excess of 2000 K. EUV photons evaporate only the smallest grains with sizes less than 6\AA (Jochim *et al.* 1994).

5. ENERGY DISTRIBUTIONS

Bland-Hawthorn & Voit (1993) examine the influence of three different ionizing continua: a simple power law and thermal bremsstrahlung spectra at temperatures of 0.2 and 5 keV. Here, we restrict our attention to a power law and a more realistic ‘quasar spectrum’ incorporating a ‘big blue bump’ (e.g.

Sanders *et al.* 1989). For the latter, we define

$$\mathcal{L} = k_1 \varepsilon^{-2/3} \exp[-\varepsilon/\varepsilon_1] + k_2 \varepsilon^{-\alpha} \exp[-\varepsilon/\varepsilon_2] \mathcal{H}(\varepsilon - \varepsilon_1) \quad (3)$$

in units of photons per second per unit energy integrated over the accretion disk, for which \mathcal{H} is the Heaviside operator. The first term represents the ‘cool’ accretion disk which produces the big blue bump, for which the spectrum turns over at $\varepsilon_1 = 30$ eV (Fig. 5a). The second term represents the influence of the ‘hot’ disk and corona, where the spectrum with slope $\alpha = 1.9$ turns over at $\varepsilon_2 = 100$ keV. In practice, ε_2 can be as high as 400 keV (Dermer & Gehrels 1995). The ratio of total energy radiated from the hot and cool regions, ρ , is obtained from

$$k_2 = \frac{L_{\text{tot}} \varepsilon_2^{2-\alpha}}{(1+\rho)} \left(\Gamma(2-\alpha) - \frac{(\varepsilon_1/\varepsilon_2)^{2-\alpha}}{(2-\alpha)} + \frac{(\varepsilon_1/\varepsilon_2)^{3-\alpha}}{(3-\alpha)} \right)^{-1} \quad (4)$$

where Γ is the Gamma function and L_{tot} is the total luminosity from integrating equation 3 with respect to energy. For our quasar nucleus, we adopt $\rho = 10$.

The most crucial parameter in Voit’s models is the x-ray flux incident on the molecular cloud, $F_{\text{in}} = \int f_\nu d\nu$. We consider flux levels of $10^8, 10^4$ and 10^2 erg cm⁻² s⁻¹ equivalent to placing a molecular cloud at distances of 1 pc, 100 pc and 1 kpc respectively from a 10^{46} erg s⁻¹ ionizing source. Further, we consider flux levels of 10, 1 and 0.1 erg cm⁻² s⁻¹ for a cloud at 1 kpc from ionizing sources of $10^{45}, 10^{44}$ and 10^{43} erg s⁻¹ respectively. The re-radiated ionizing flux is given by

$$F_{\text{out}} = \kappa (\Delta\Omega/4\pi) \int_{\nu_0}^{\nu_1} f_\nu (1 - e^{-\sigma_\nu N_H}) d\nu \quad (5)$$

where κ is the sky coverage fraction within the total solid angle $\Delta\Omega/4\pi$ subtended by the molecular clouds, as seen from the nucleus. If we assume a cylindrical geometry, the molecular gas coincident with the $10.8\mu\text{m}$ emission lies within $\Delta\Omega/4\pi = 0.1$; the enclosed mass of gas is roughly $1.5 \times 10^9 M_\odot$ with a mean density of 120 cm^{-3} . Here, we assume that giant molecular clouds #18–24 (Planesas *et al.* 1991) lie within a cylinder of length 1.2 kpc and diameter 340 pc, such that the projected column density seen from Earth is the same as that seen by the AGN.

6. MODEL RESULTS

In Fig. 5b, we show the predicted spectra (solid lines) from a simple power law where the limits of integration in equation 5 are taken to be $\nu_0 = 100$ eV/h and $\nu_1 = 10$ keV/h. The re-radiated spectrum is a strong function of the x-ray flux incident on the molecular gas; the spectral shape is of secondary importance. The far-infrared emission provides a strong constraint on an x-ray heating model: e.g., a flux of $40 \text{ erg cm}^{-2} \text{ s}^{-1}$ can explain the $10.8\mu\text{m}$ emission at the expense of predicting too much far-infrared emission. A flux level of $10 \text{ erg cm}^{-2} \text{ s}^{-1}$, equivalent to putting all of the bolometric luminosity within our x-ray band, falls short by an order of magnitude in explaining the mid-infrared emission.

There are two ways in which the re-radiated mid-infrared emission can be enhanced at the expense of the far-infrared emission. First, if a significant fraction of small grains ($\leq 10\text{\AA}$) are able to survive, their broad temperature distributions, while undergoing thermal transients, can selectively enhance the near-infrared flux. Secondly, the models discussed so far do not include a direct UV component, nor do the

models consider the UV and optical emission expected to arise in the gas phase around the x-ray heated grains. To address the role of a more realistic quasar spectrum, we adopt the form in equation 3 (Fig. 5a) over the interval 10 eV to 10 keV. The form of the ionizing continuum falls within the observed range (Pier *et al.* 1994, Fig. 3), except beyond 2 keV where the observed x-ray spectrum turns up. The predicted far infrared spectra are illustrated with dashed lines in Fig. 5b.

At a flux level of $30 \text{ erg cm}^{-2} \text{ s}^{-1}$, such a model could reasonably explain the $10.8\mu\text{m}$ detection at the same time as falling within the limits imposed by the IRAS measurements. The necessary EUV ionizing luminosity is $3L_{45} \text{ erg s}^{-1}$, where L_{45} is the nuclear luminosity in units of $10^{45} \text{ erg s}^{-1}$, a factor of five larger than that inferred by Pier *et al.* (1994) for the bolometric nuclear flux.

The $25\mu\text{m}$ IRAS measurement poses a challenge for the ‘buried quasar’ model. However, an enhanced blue component is borne out by the ISO observations of the narrow-line region for a wide range of ionic species within the $2 - 40\mu\text{m}$ window. The range in ionization potentials (30–300 eV) lead Lutz *et al.* (1997) to infer a strong enhancement at EUV wavelengths. The additional ionizing flux we need from the nucleus could be reduced, and the $25\mu\text{m}$ IRAS constraint made less stringent, if much of the UV is produced by hot young stars at the nucleus or embedded within the CO arms.

There is always the possibility of autoionizing shocks driven by a powerful $\sim 10^{56} \text{ erg}$ wind associated with the radio jet. In Fig. 3a, we note that the base of the NE [OIII] plume radiates strongly in [NII] emission, and only weakly at $\text{H}\alpha$. This situation routinely arises in the presence of fast shocks (Dopita & Sutherland 1995). But in support of AGN photoionization of the narrow-line region, Marconi *et al.* (1996) note that the infrared [SiIX]/[SiVI] line ratio is very much higher than observed in planetary nebulae and in gas surrounding hot young stars.

The factor κ in equation 5 allows for clumpiness within the solid angle seen from the nucleus. For a typical AGN spectrum, F_{out} will depend much more sensitively on κ than on N_H at column densities of 10^{23} cm^{-2} . By way of example, if we take $\kappa = 0.3$, increasing N_H by a factor of 3 allows the cloud to absorb the x-ray power between about 3 keV and 5 keV, but this is a small fraction of the total power. In the present models, we do not consider self-absorption of the near- to mid-infrared emission by the dusty medium. The details of this correction depend on the cloud-source geometry and obviously depends on whether we are viewing the irradiated or back surface of the molecular cloud. For the measured column density, this is more critical for the K band where the extinction correction is expected to be $\sim 10 \text{ mag}$ compared to $\sim 0.1 \text{ mag}$ at $\lambda 10\mu\text{m}$.

7. INFRARED EMISSION FROM SMALL GRAINS?

As noted by Wynn-Williams *et al.* (1985), an alternative explanation is $\lambda\lambda 3.3 - 11.3\mu\text{m}$ line emission from PAH molecules (e.g. Molster *et al.* 1996). However, for the x-ray fluxes considered in our models, PAH grains should be destroyed (Voit 1992; Bland-Hawthorn & Voit 1993). To test this idea, the SW $11\mu\text{m}$ plume was observed in the L band on 1995 July 16 with the UKIRT CGS4 infrared spectrometer at a resolving power of 700. The InSb array gave $1''.5$ pixels and the entrance slit projected to $3'' \times 90''$. The exposure time was 90 sec over an elapsed time of 40 mins due to overheads in beam switching every 20 sec. The data, presented in Fig. 4, were flux calibrated using BS 859 (A7 IV star). Similar experiments were carried out with the CASPIR infrared spectrometer at MSO 2.3m and at $10\mu\text{m}$ with CGS3 at UKIRT although the data have lower signal to noise. The measured flux at $3\mu\text{m}$ is shown in Fig. 5b, multiplied by

a factor of two to account for both plumes. The K measurement was obtained from data supplied by H. Thronson after subtracting the stellar bar; the 10.8μ measurement is from Telesco & Decher (1988).

In Fig. 4, while weak continuum is detected in the SW $11\mu\text{m}$ plume, there is only a suggestion of a broad, weak $3.3\mu\text{m}$ PAH feature. In contrast, the nuclear spectrum shows a strong narrow feature near the expected wavelength for PAH emission bracketted by broad C-H absorption features. However, it is not at all clear that this is the correct identification. The Infrared Space Observatory (ISO) has shown that PAH features have broad bases ($\sim 0.1\mu\text{m}$) which are not seen in our nuclear spectrum (Molster *et al.* 1996). Moreover, strong PAH emission is always observed in star forming regions (e.g. Acosta-Pulido *et al.* 1996) and rarely seen near AGNs (Roche *et al.* 1991; cf. Mazzarella *et al.* 1994). The emerging picture is that both EUV (Jochim *et al.* 1994; Allain *et al.* 1996a) and x-ray radiation (Voit 1992) destroy small (PAH) grains, although EUV photons only wipe out grains with less than 50 carbon atoms ($a < 6\text{\AA}$; Omont 1986). Star-forming regions are strong PAH emitters because the EUV flux is rapidly attenuated by the neutral gas, leaving sub-ionizing photons to heat the small grains. *To remove all PAH-type grains requires x-rays.*

Voit (1992) has laid down strict requirements for PAH survival in the presence of x-rays where PAHs are assumed to rebuild themselves as efficiently as possible. The critical ionization parameter U^{CR} (number density of photons to gas atoms) is 10^{-4} above which all PAH structures are destroyed; this important limit is even lower if the PAHs are primarily ionized (Allain *et al.* 1996b). At a distance of 1 kpc, $U^{\text{CR}} \sim 0.1L_{45}$ for a mean gas density of $n_H = 10^2 \text{ cm}^{-3}$. Thus, an x-ray luminosity of $L_X \sim 10^{42} \text{ erg s}^{-1}$ is the minimum requirement for grain destruction but only within a column of 10^{22} cm^{-2} (Voit 1992; eq. 7 and Fig. 3). For L_X a factor of ten higher, most of the PAH emitters are expected to be wiped out.

Towards the nucleus, the C-H features indicate $A_V \approx 22$ (Bridger *et al.* 1994) but this corresponds to an optical depth of unity in the L band ($N_H \sim 4 \times 10^{22} \text{ cm}^{-2}$). If the nuclear line at $\lambda 3.3\mu\text{m}$ is indeed due to PAH grains, we suspect that these regions are shielded from the central accretion disk by much higher columns of obscuring material or by shadowing in a highly inhomogeneous medium. If the PAH emission is produced in gas with $n_H \sim 10^6 \text{ cm}^{-3}$ at a distance of 30 pc from the nucleus, a shielding column of 10^{24} cm^{-2} – presumably from the torus – is sufficient to block most of the x-rays.

8. THE ROLE OF THE NUCLEAR IONIZING LUMINOSITY

The Ringberg workshop constitutes a major landmark in the study of active galactic nuclei. The VLBA imaging (Gallimore *et al.* 1997) and the most recent water maser results (Greenhill & Gwinn 1997) appear to suggest that the accretion disk about the central black hole (radio source S1) is warped on parsec scales. This was originally proposed by Phinney (1989a,b) to explain the observation that the ionizing cones and radio axes in Seyferts are randomly oriented with respect to the rotation axes of the host galaxy. The newly discovered radiation-driven warping instability would seem to provide the most promising explanation for misalignments on parsec scales (Pringle 1996). An optically thick, planar disk (to both absorption and emission), illuminated by a compact radiation source at its center, is unstable to warping under the action of radiation pressure.

Maser kinematics suggest that the mass of the central black hole is $1 - 2 \times 10^7 M_\odot$, implying that the nuclear bolometric luminosity of $0.6L_{45} \text{ erg s}^{-1}$ (Pier *et al.* 1994) is roughly half the Eddington limit ($1 - 2L_{45} \text{ erg s}^{-1}$). If a warped accretion disk removes the need for a torus (Begelman 1997), there are presently no reliable constraints on the unobscured ionizing flux. The $11\mu\text{m}$ plumes suggest that the

intrinsic EUV luminosity could be significantly higher ($3L_{45}$ erg s⁻¹) than the value inferred by Pier *et al.* (1994). Pier attempts to infer the scattered fraction of nuclear radiation in order to arrive at the true nuclear luminosity, which leads to uncertainties of a factor of two. The nuclear luminosity inferred from the 11 μ m emission could be lowered by as much as 50% if one considers the possible role of stellar heating (§3). Thus, our luminosity and that of Pier may be marginally consistent. For either value, it seems that radiation pressure is likely to be important, at least in the innermost accretion flow, and the accretion rate could be at super-Eddington levels. The expected anisotropy of radiation from a super-Eddington accretion flow (Sikora 1981) could conceivably account for the degree of intrinsic beaming required by the PAH emission and mid-IR reprocessed radiation.

In earlier papers, we demonstrated that the inner 10 kpc disk of NGC 1068 displays an isotropic, diffuse ionized medium with an implied cooling rate of $0.2 L_{45}$ erg s⁻¹ (Bland-Hawthorn *et al.* 1991*a*, *b*). Sokolowski *et al.* (1991) contend that the same electron-scattering medium which gives rise to both the observed x-ray spectrum and the polarized broad-line spectrum can produce a dilute, hard ionizing continuum that is sufficiently energetic to power the low ionization emission. Halpern (1992) suggests that the extended x-ray disk observed by ROSAT (Wilson *et al.* 1992) may not be sufficient to balance the cooling rate of the DIM, and reiterates that the active nucleus could be an important source of ionizing radiation. A nuclear EUV luminosity as high as $3L_{45}$ erg s⁻¹ would be sufficient to power the diffuse component. However, the lower value of Pier *et al.* (1994) requires a different source, presumably the extended disk. Thus, establishing the true nuclear ionizing luminosity has important consequences on all scales within NGC 1068.

9. CONCLUSIONS

The lack of PAH features in the SW 11 μ m plume probably indicates that the x-ray flux at the distance of the CO arms is at least 0.1 erg cm⁻² s⁻¹ which requires a nuclear x-ray luminosity of more than 10^{43} erg s⁻¹. Since the observed luminosity is an order of magnitude smaller (Monier & Halpern 1987), the scattered x-rays are insufficient to wipe out PAH grains from molecular clouds outside of the ionizing cones. But future observations with better sensitivity could show weak PAH features within the ionization cones, and these would require a detailed understanding of the radiation transfer through the molecular clouds.

If the jet-axis molecular clouds are primarily heated by the nucleus, the infrared spectrum of the 11 μ m plumes indicates an unobscured EUV ionizing luminosity as high as 3×10^{45} erg s⁻¹, although this value could be reduced by up to 50% if stellar heating is also important within the jet-axis molecular clouds. For a typical ‘blue bump’ to x-ray energy ratio of 30 (Sanders *et al.* 1989), the unobscured x-ray luminosity would be 10^{44} erg s⁻¹. The observed scattered x-rays would therefore require a Thompson depth, $\tau_e = 0.01$, in rough agreement with theoretical models (q.v. Pier *et al.* 1994).

ACKNOWLEDGMENT. The authors are indebted to E.A. Pier and D. Lutz for invaluable comments on an earlier manuscript.

REFERENCES

Acosta-Pulido, J.A. *et al.* 1996, A&A, 315, L121

- Allain, T. *et al.* 1996*a*, A&A, 305, 602
- Allain, T. *et al.* 1996*b*, A&A, 305, 616
- Antonucci, R.R.J. & Miller, J.S. 1985, ApJ, 297, 621
- Begelman, M.C. 1997, ApSS, in press
- Bergeron, J., Petitjean, P. & Durret, F. 1989, A&A, 213, 61
- Bland-Hawthorn, J. *et al.* 1997, ApSS, in press
- Bland-Hawthorn, J., Sokolowski, J. & Cecil, G. 1991, ApJ, 375, 78
- Bland-Hawthorn, J. & Voit, G.M. 1993, Rev. Mex. Astron. Ap, 27, 73
- Bridger, A., Wright, G.S. & Geballe, T.R. 1994, In McLean, I., ed., Infrared Astronomy with Arrays, Kluwer, Dordrecht, 537
- Brown, & Gould, 1976, Phys. Rev. D1, 2252
- Cecil, G., Bland, J. & Tully, R.B. 1990, ApJ, 355, 70
- Condon, J.J. & Yin, Q.F. 1990, ApJ, 357, 97
- Dermer, C.D., & Gehrels, N. 1995, ApJ, 447, 103
- Dopita, M.A. & Sutherland, R. 1995, ApJ, 455, 468
- Evans, I.N. & Dopita, M.A. 1986, ApJ, 310, L15
- Gallimore, J.F., Baum, S.A., O’Dea, C.P. & Pedlar, A. 1996, ApJ, 458, 136
- Gallimore, J.F. *et al.* 1997, ApSS, in press
- Greenhill, L. & Gwinn, C.R. 1997, ApSS, in press
- Halpern, J. 1991, In Testing the AGN Paradigm, eds. Holt, Neff, Urry, p. 524.
- Jochims, H.W. *et al.* 1994, ApJ, 420, 307
- Lutz, D. *et al.* 1997, ApSS, in press
- Mathis, J.S., Rumpl, W. & Nordsieck, K.H. 1977, ApJ, 217, 425
- Mazzarella, *et al.* 1994, AJ, 107, 1274
- Molster, F.J. *et al.* 1996, A&A, 315, L373
- Monier, R. & Halpern, J. 1987, ApJ, 315, L17
- Neff, S.G. *et al.* 1994, ApJ, 430, 545
- Omont, A. 1986, A&A, 164, 159
- Phinney, S. 1989*a*, ApJ, 347, 29

- Phinney, S. 1989*b*, In Theory of Accretion Disks, eds. F. Meyer, W. Duschl, J. Frank, E. Meyer-Hofmeister (Dordrecht: Kluwer), 457
- Pier, E.A., Antonucci, R., Hurt, T., Kriss, G. & Krolik, J. 1994, ApJ, 428, 124
- Planesas, P., Scoville, N.Z., & Myers, S.T. 1991, ApJ, 369, 364
- Pogge, R.W. 1988, ApJ, 328, 519
- Puget, J.L. & Leger, A. 1989, ARAA, 27, 161
- Roche, P.F., Aitken, D.K., Smith, C.H. & Ward, M.J. 1991, MNRAS, 248, 606
- Sanders, D.B. *et al.* 1989, ApJ, 347, 29
- Scoville, N.Z., Matthews, K., Carico, D.P. & Sanders, D.B. 1989, ApJ, 327, L61
- Shopbell, P.L. & Bland-Hawthorn, J. 1997, ApJ, in press
- Sikora, M. 1981, MNRAS, 196, 257
- Sokolowski, J., Bland-Hawthorn, J. & Cecil, G.N. 1991, ApJ, 375, 583
- Telesco, C.M., Becklin, E.E., & Wynn-Williams, C.G. 1980, ApJ, 241, L69
- Telesco, C.M. & Decher, R. 1988, ApJ, 334, 573
- Thronson, H.A. *et al.* 1989, ApJ, 343, 158
- Thronson, H.A., Campbell, M.F., & Harvey, P.M. 1979, AJ, 83, 1581
- Voit, G.M. 1991, ApJ, 379, 122
- Voit, G.M. 1992, MNRAS, 258, 841
- Wilson, A.S., Elvis, M., Lawrence, A., & Bland-Hawthorn, J. 1992, ApJ, 391, L75
- Wynn-Williams, C.G., Becklin, E.E., & Scoville, N.Z. 1985, ApJ, 297, 607

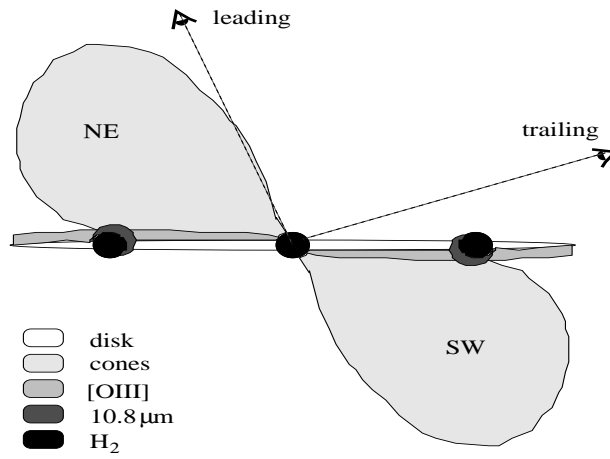


Fig. 1.— Schematic drawing of NGC 1068 in side elevation showing the orientation of the ionization/radio jet cones to the line of sight. If the spiral arms trail, the northern half of the disk falls behind the plane of the sky; if the spiral arms lead, the southern half falls behind. For either orientation, the NE cone lies in front of the disk, and the SW side behind the disk.

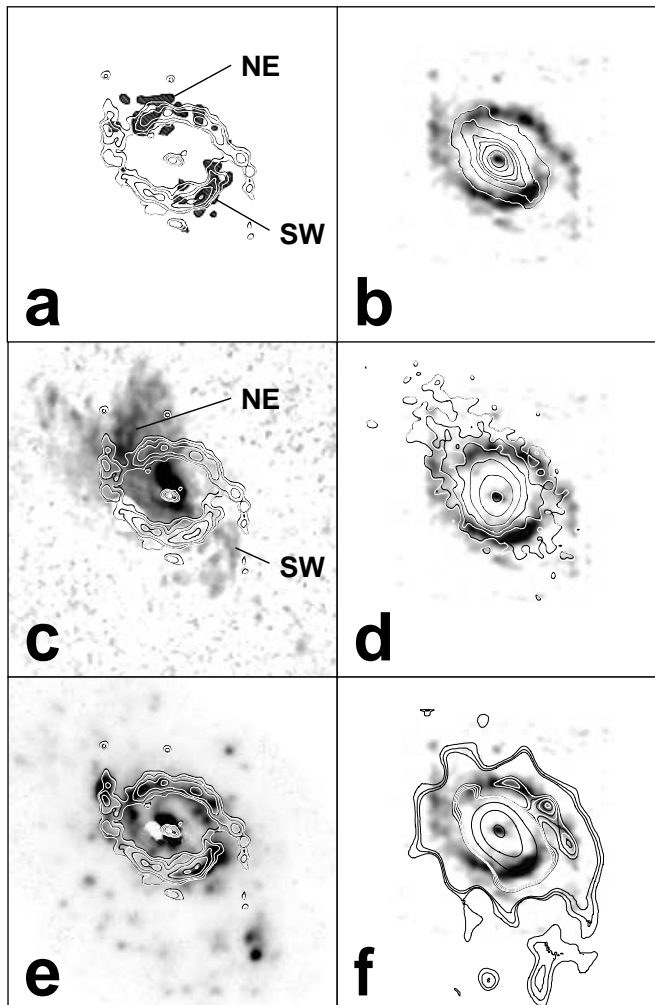


Fig. 2.— A collage of multi-band observations over the inner $145''$ of NGC 1068 superimposed on CO($J=1-0$) line observations (Planesas *et al.* 1991) in contours (*a*, *c*, *e*) and in half tone (*b*, *d*, *f*). All maps are presented at $4''$ FWHM resolution except for the $H\alpha$ and [OIII] data shown at $1''$ FWHM resolution. In (*a*), the hatched regions are the $10.8\mu\text{m}$ emission observed by Telesco & Decher (1988), i.e. the NE and SW $11\mu\text{m}$ plumes. In (*b*), the K band continuum from Thronson *et al.* (1989), shown with contours, reveals the central stellar bar. In (*c*), the half tone image is the [OIII] $\lambda 5007$ line flux from observations with the Rutgers Fabry-Perot (the SE hole is an excised ghost). The NE and SW plumes do not coincide with the $11\mu\text{m}$ plumes. In (*d*), the contours are the ROSAT (0.1–2.4 keV) HRI data (Wilson *et al.* 1994), where the flux is shared roughly between a point source and an extended (mostly NE) region. In (*e*), the half tone image reveals a dense distribution of HII regions in close association to the molecular gas. In (*f*), the contours are the VLA $\lambda 6\text{cm}$ data (Wynn-Williams *et al.* 1985): the NW radio ‘plateau’ is resolved into a ridge coincident with the CO emission.

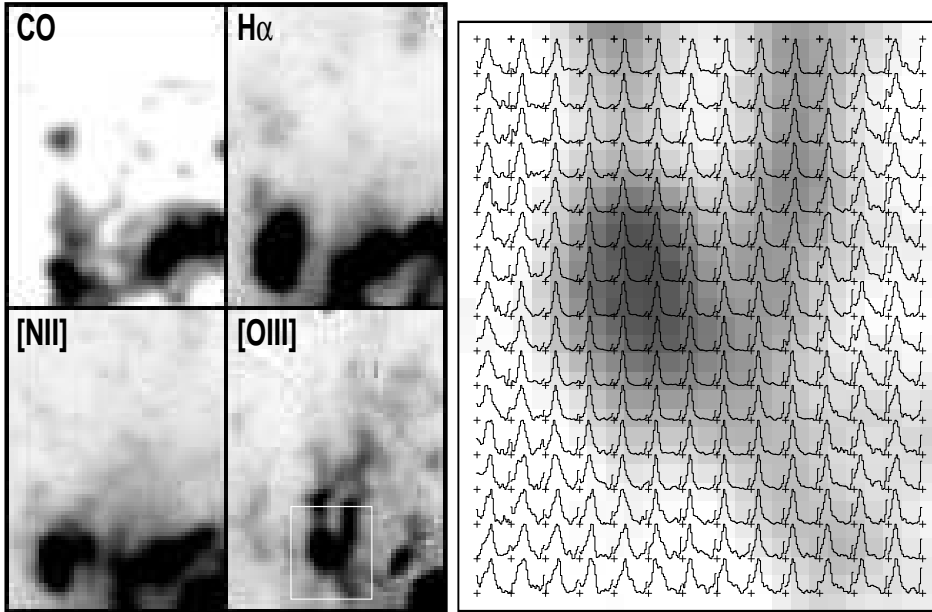


Fig. 3.— *Left:* (a) A comparison of the CO($J=1-0$), [OIII], $H\alpha$ and [NII] flux in the NE [OIII] plume. *Right:* (b) The width of the [OIII] line profiles at the base of the plume correlates with the total line flux (shown in half tone) in the sense that the lines get broader as the flux decreases. Crosses indicate pixels binned 2×2 . The region shown is indicated by the white box in (a).

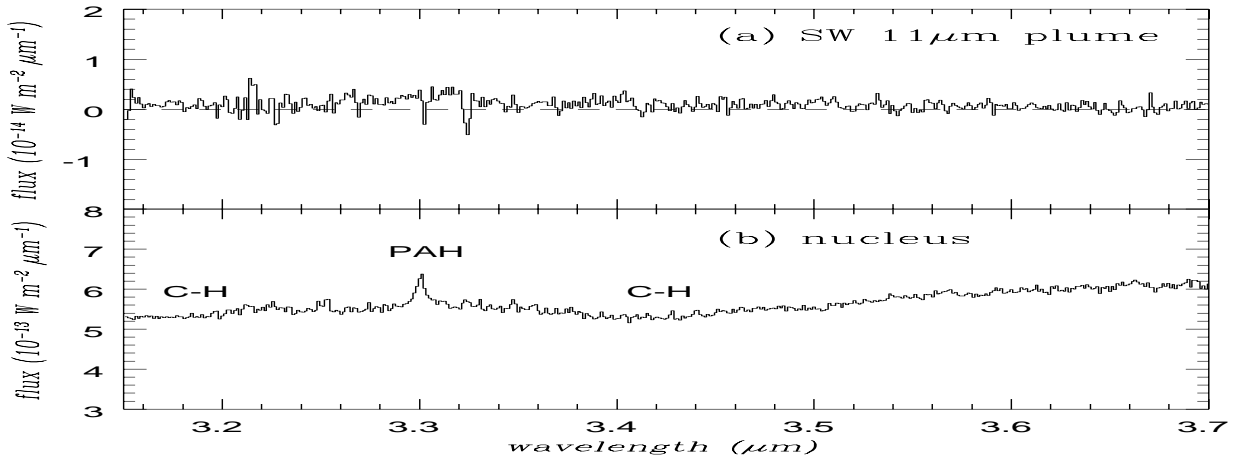


Fig. 4.— CGS4 spectra of the SW $11\mu\text{m}$ plume and the nucleus in NGC 1068. (a) The identification of a nuclear PAH feature is uncertain (see text). The C-H features indicate high absorption columns ($A_V \sim 20$) towards the nucleus. (b) In addition to a weak continuum, there is a suggestion of weak PAH emission (broad base) in the SW plume.

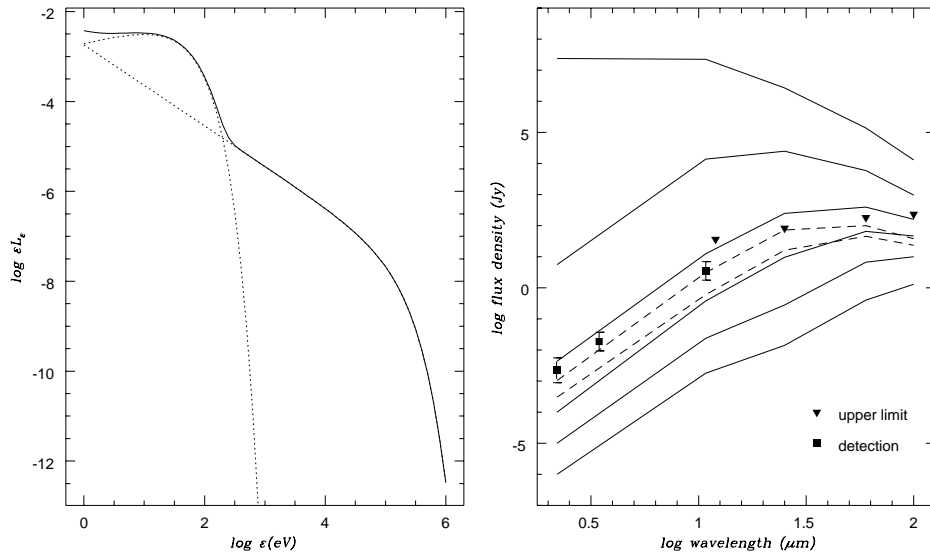


Fig. 5.— *Left.* (a) Bolometric spectrum from the accretion disk model where the total energy been normalized to unity. The ‘big blue bump’ turns over at 30 eV; the hard energy component turns over at 100 keV. *Right.* (b) The predicted near- to far-infrared spectra for the MIR features. The solid lines are computed from the power-law models with flux levels of 10^8 , 10^4 , 10^2 , 10, 1, 0.1 $\text{erg cm}^{-2} \text{s}^{-1}$ (top to bottom). The filled triangles indicate upper limits for the $11\mu\text{m}$ plumes from IRAS measurements. The filled squares are the detections discussed in §7. The dashed lines correspond to flux levels of $10^{1.5}$ and 10 $\text{erg cm}^{-2} \text{s}^{-1}$ and include a quasar-like ‘big blue bump’ component.